The role of adhesive in the mechanical response of adhesively bonded aluminum hat sections under axial compression

Jianping Lu, Golam M. Newaz *, Ronald F. Gibson

Department of Mechanical Engineering, Wayne State University, 5050 Anthony Wayne Drive, Detroit, MI 48202, USA

Abstract

Aluminum hat sections, either adhesively bonded or unbonded, experience buckling, post-buckling and plastic collapse when axially compressed. However, there exist obvious differences in the load–displacement response between the bonded and unbonded hat sections. Finite element eigenvalue buckling analysis is carried out to predict the buckling load and mode. Experiments show that when adhesively bonded hat sections begin to buckle there is a transformation from the 1st buckling mode to the higher ones, while the unbonded hat sections develop the post-buckling based on the lowest buckling mode. The different buckling modes result in not only different buckling loads but different peak loads of the hat sections as well. Finally, ultimate compressive strength formulae are proposed for hat sections.
© 2004 Elsevier Ltd. All rights reserved.

Keywords: Aluminum and alloys; Finite element stress analysis; Stress analysis; Stress distribution

1. Introduction

When hat sections are axially compressed with sufficiently large loads, buckling occurs. The buckling load can be computed according to the extremely involved formulae by Bulson (1969), or a simpler formula by Becker (1957) with a coefficient given graphically. The influence of joint types (spot-welded or weld-bonded) on the axial impact performance of aluminum hexagonal box section was investigated (McGregor et al., 1990), and the adhesive with a higher toughness was found to resist the bondline peel better than the adhesive with a lower toughness. But the unbonded case was not addressed and the role of the adhesive was not discussed in depth. Adhesively bonded steel box beam sections with a variety of geometrical combinations were tested to verify the impact performance and to provide design guidelines. Again, the role of the adhesive was not studied (Fay and Suthurst, 1990). In the weld-bonded joint, when both normal and shear

* Corresponding author. Tel.: +1-313-577-3877; fax: +1-313-577-8789.
E-mail address: gnewaz@eng.wayne.edu (G.M. Newaz).

L = 100 mm, A= 50 mm
B=25 mm, t = 1 mm
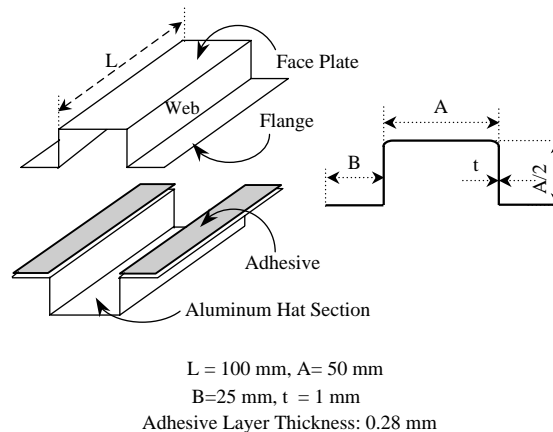Adhesive Layer Thickness: 0.28 mm

Fig. 1. Geometrical dimensions of the hat section.

stresses are considered, the elastic modulus of the adhesive material and the thickness of the adhesive layer are believed to influence the stress distribution in the whole lap region (Lee and Kong, 2000).

Given the lack of information on the role of the adhesive in buckling response of hat sections, the primary objectives of this research activity were:

1. To experimentally determine the buckling load, buckling modes and ultimate strength of the adhesively bonded and unbonded hat sections and understand the different load responses between the bonded and unbonded cases.
2. To predict the buckling load and the relative buckling mode for the bonded and unbonded hat sections using finite element eigenvalue buckling analysis and propose an empirical formula to estimate the ultimate compressive strength of the adhesively bonded and unbonded hat sections.

In the present study, two aluminum hat sections are bonded together through the flanges to form a box-section (Fig. 1). It was expected that with a specific brittle adhesive the hat sections would be strengthened and the adhesive bonding would absorb a significant amount of energy during the compression due to either adhesive material failure or interface debonding, since the shear stress in the adhesive and the peeling stress at the interface should be fairly high when bondline fracture begins. Hence, the global load response of the bonded hat sections should be higher than that of the unbonded hat sections.

2. Experiments on axial compression

2.1. Compression tests

The materials used to construct the adhesively bonded (or unbonded) aluminum hat sections are Al 6111-T4 and Dow Betamate® 4601 structural adhesive. When the specimens were prepared, no surface preparation was used in order to be consistent with automotive industry practice. The thickness of the bondline is automatically controlled by glass beads (0.28 mm in diameter) which are mixed in the adhesive. For a thin rectangular plate under compression loading, the edge constraint condition effect on the buckling strength is less significant with large plate aspect ratio than the small plate aspect ratio. Therefore, a plate aspect ratio of 2 for the face plate (shown in Fig. 1) was adopted in this research attempt, and the

Table 1
Material properties of aluminum and adhesive

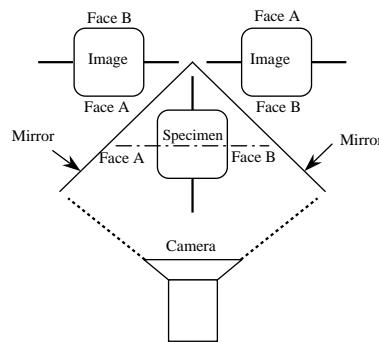| Materials	Young's modulus (GPa)	Poisson's ratio	Yield stress (MPa)
Al 6111-T4 aluminum alloy	69	0.3	175
Betamate® 4601	3.6	0.26	40

Fig. 2. Image capture device.

methodology can be extended to longer hat sections without much change. The geometrical dimensions of the hat section are shown in Fig. 1. The material properties of the two materials are listed in Table 1.

Tests were conducted to first determine which plate element in the hat sections buckles first, and as soon as a plate element buckles the hat sections should be regarded as buckled also. Secondly, the tests were used to collect the history of the total load applied to the hat sections and the buckling mode shapes. Because the two flange parts of a hat section are symmetric, it is therefore only necessary to observe one of these flanges and the two face plates in the test. A special image capture device (shown in Fig. 2) was used to simultaneously observe the buckling of all these surfaces with one camera.

The compression tests were conducted using a servo-hydraulic MTS 810 machine with an automated data acquisition system connected to a time-based medium speed image acquisition system (shown in Fig. 3). The hat sections were centered on the bottom test platen, and the lower platen moved up until the set displacement was reached. Considering the small amount of displacement before the peak load, a total of 2 mm axial displacement was set to capture the buckling deformation and peak load point, and the loading rate was 1 mm/min. For the entire collapse load response history of the bonded and unbonded hat sections, a 20 mm axial displacement was imposed. During the tests, three channels of data were recorded for each test e.g., time, load and displacement. The images were then analyzed to accurately determine the instant when buckling occurred. The buckling load and the peak load were determined from the recorded data accordingly. For each hat section type, four specimens were tested.

2.2. Post-buckling stress distribution on plate elements

Peery (1949a,b,c) reported that when a flat plate simply supported at all four edges is loaded at one edge by a rigid block, the compression stresses are uniformly distributed along the loading edges if the load is smaller than the buckling load even though the stress values increase as loading progresses. When the load is greater than the buckling load, the stress distribution changes in such a way that near the middle of the cross-section the stress remains approximately equal to the buckling stress, meanwhile, at the sides of the sheet, buckling is prevented because the sides of the sheet must remain straight and consequently must be
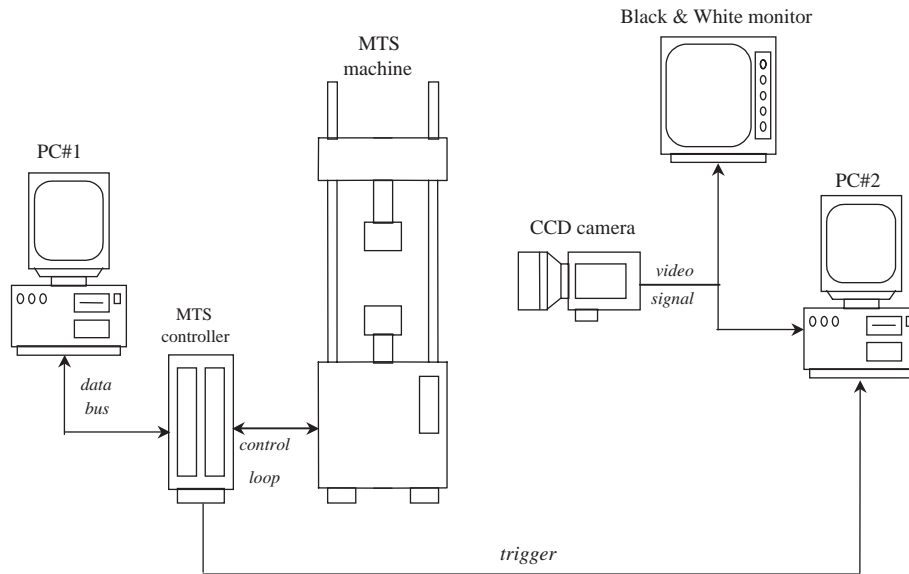
Fig. 3. Compression test MTS system setup.

stressed in proportion to the strain in the direction of loading so that the stress level is much higher than in the middle.

Typically, the plate elements in the hat sections do not buckle at the same time due to width or thickness variations. Moreover, the flanges have one edge free. Therefore, for the hat sections, the boundary conditions are much more complicated than all simply supported edges. Also, there are bending moments between two adjacent plate elements in the post-buckling stage and the common edges are no longer straight. The classical assumption based formula used to calculate the ultimate compressive strength of a single plate element has to be modified to become applicable to the whole hat section.

SPI Pressurex® pressure indicating sensor film was used to measure the contact pressure distribution between the loading end of the hat section and the platen of the MTS machine. The Pressurex® film was placed between the top end of the hat section and the platen, and then loaded. After the film was removed, it immediately revealed the pressure distribution profile by the color intensity. Generally, the accuracy is within 10% by visual comparison with the color correlation chart.

3. Finite element eigenvalue buckling stress analysis

Finite element eigenvalue buckling analysis was performed to predict the buckling modes and relevant buckling loads for the bonded and unbonded hat sections. Usually, only the buckling mode related to the lowest buckling load is considered. But, when there is a mode transformation, all the buckling modes with buckling load lower than the elastic limit should be taken into account.

The eigenvalue buckling analysis was carried out using the ABAQUS code. In the finite element context, the classical eigenvalue buckling problem may be stated as follows. Given a structure with an elastic stiffness matrix, $K_{(b)}^{NM}$, a loading pattern defined by the vector Q^M, and an initial stress and load stiffness matrix, $K_{(Q)}^{NM}$, find load multipliers (eigenvalues), λ_i, and buckling mode shapes (eigenvectors), ϕ_i^M, which satisfy
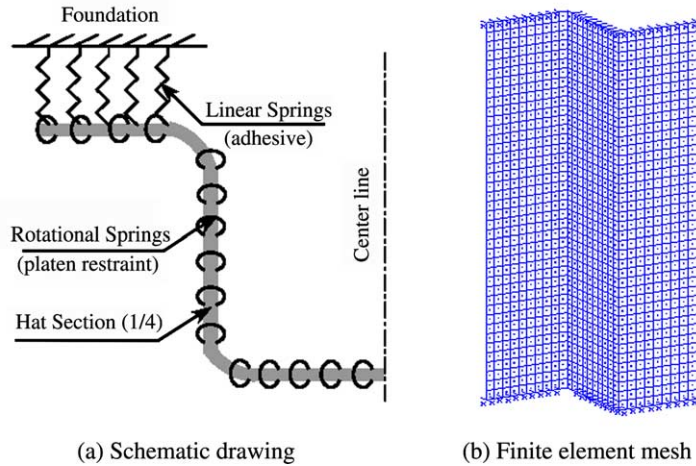
Fig. 4. Finite element modeling of the hat sections.

$$[K_{(b)}^{NM} + \lambda_i K_{(Q)}^{NM}]\phi_i^M = 0 \tag{1}$$

The critical buckling loads are then given by $\lambda_i Q^M$. In the above, the superscripts N and M change from 1 to the degree of freedom of the whole model, and the subscript i refers to the ith buckling mode.

The hat section was modeled by S4R 3D shell elements. Experiments showed that in the bonded case the flanges do not have apparent elastic buckling deformation so that the adhesive material can be modeled by a group of linear springs with one end fixed in the foundation and the other end connected to the aluminum flange as shown in Fig. 4. The spring constant ($k = 78.4 \times 10^6$ N/m) was determined by the adhesive material's Young's Modulus. The disadvantage of this approach is that the stresses in the adhesive layer cannot be determined and adhesive failure cannot be predicted, but for buckling predictions it should be adequate. The unbonded case can be realized by letting the linear spring constant be zero. Uniform edge pre-load was applied to the top of the hat section, while the bottom of the hat section was constrained in the loading direction. Because the loading platen exerts rotational constraint to the ends of the hat sections, elastic restraint was implemented by using a group of rotational springs on both ends of the hat section model (Fig. 4). In order to simplify the analysis, a spring constant $k = 5000$ (N m/Rad) was used for all the rotational springs.

4. Ultimate strength of the hat sections

It has been found (Von Karman et al., 1932) that when a rectangular plate with all four edges simply supported is under axial compression, it can be assumed that the total load is carried finally by two strips of width c, and that the load distribution is uniform across these strips. Then the middle portion of the sheet can be disregarded and the two strips can be handled as a long simply supported rectangular plate of width $2c$. If this long rectangular plate becomes a square one, the critical buckling stress for such a plate is (Timoshenko, 1936a,b,c)

$$\sigma_{cr} = \frac{\pi^2 E t^2}{12(1 - v^2)c^2} \tag{2}$$

where, E is the Young's modulus; t, plate thickness; v, Poisson ratio.

Assuming that the ultimate load is reached when σ_{cr} becomes equal to the yield point stress σ_y of the material, it can be found from (2) that

$$c = \frac{\pi t}{\sqrt{12(1-v^2)}} \sqrt{\frac{E}{\sigma_y}} \tag{3}$$

If we put Poisson's Ratio $v = 0.3$, the effective width in Eq. (3) can be written as

$$c = 0.95t \sqrt{\frac{E}{\sigma_y}} \tag{4}$$

and the ultimate load is

$$P_{ult} = 2ct\sigma_y = \frac{\pi t^2}{\sqrt{3(1-v^2)}} \sqrt{E\sigma_y} \tag{5}$$

Attention needs to be paid when using the above formulae. The critical stress in Eq. (2) reflects only the lowest buckling mode that is anti-symmetric, and when higher buckling modes are dealt with the expression for the critical buckling stress should be rewritten even though in most cases it is not explicitly available.

In the above expression for P_{ult}, it is seen that the ultimate load is independent of the width of the plate and is just proportional to the square of its thickness. It was pointed out by Timoshenko (1936a,b,c) that sufficient accuracy can be achieved by using the following equation

$$P_{ult} = Ct^2 \sqrt{E\sigma_y} \tag{6}$$

where C is a constant which depends on the plate material and plate proportions. A curve for C which can be used in practical calculations of ultimate strength of thin compressed sheets of metal was given (Timoshenko, 1936a,b,c).

Peery (1949a,b,c) extended the expression of the effective width c with more complicated boundary conditions such as one unloaded side simply supported and the other free, and a conservative value of effective width is recommended as

$$c = 0.60t \sqrt{\frac{E}{\sigma_y}} \tag{7}$$

However, Peery (1949a,b,c) also found that even though numerous other equations have been used, none of them provides accurate correlation with test results under all conditions. Uncertainties regarding the effects of edge restraints in the actual structures, accidental eccentricities in the sheet, and the effects of stresses beyond the elastic limit further complicate the problem.

5. Results and discussion

Compression tests indicated that in both bonded and unbonded cases the face plates are the governing plate members that began to buckle first while essentially no buckling was observed in the web plates and the flanges. The bonded hat section underwent the transformation from the 1st buckling mode to the 3rd mode on the two face plates, and the anti-symmetric 1st buckling mode occurred at the very early loading stage. Because of the stiffening effect from the flanges that kept straight until the peak load point and hence restrained the rotational displacement of the unloaded edges of the face plates, this anti-symmetric 1st buckling mode was unable to further develop. Since the compressive load kept increasing, the higher symmetric buckling mode which corresponds to a higher load occurred eventually as shown in Fig. 5. The
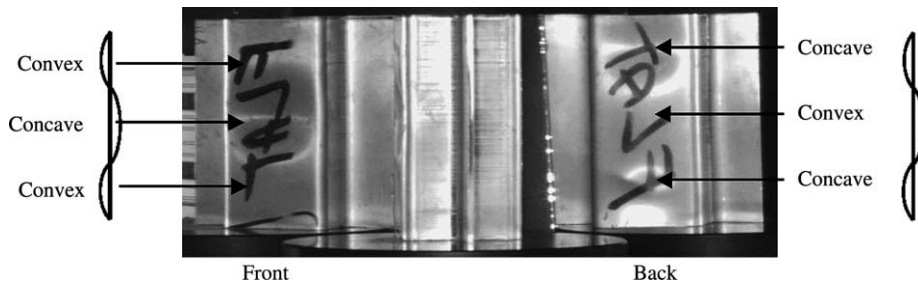
Fig. 5. The 3rd symmetric buckling mode of the bonded hat section (the arrows point to buckle locations in the front and back surface of the bonded sections).

final deformation stayed at the 3rd buckling mode because the buckling stress of the 4th mode is much higher than the elastic limit of the material so that the hat section reached its ultimate strength (peak load point) before the 4th buckling mode could occur.

For the unbonded hat sections which were simply placed together to form a box section, since the flange thicknesses are less than half of those of the bonded hat section and thus were unable to keep straight to provide necessary restraint to the rotational displacement of the face plates, the stiffening effect from the flanges was not enough to resist the development of the 1st buckling mode deformation. Consequently, no higher buckling mode was achieved in the unbonded hat sections even until the ultimate strength of the hat sections was reached as shown in Fig. 6. Also, it can be seen in Fig. 6 that there was flange separation in the unbonded case, while in the bonded case (Fig. 5), flange separation did not occur even after the peak load was reached. The experimental buckling characteristics and the ultimate strengths from the compression tests for both bonded and unbonded hat sections are listed in Table 2.

Fig. 7 shows the experimental load–displacement response comparison between the adhesively bonded and unbonded hat sections under axial compression up to a displacement of 20 mm. Even though there were load level differences between any two samples of the same hat section type, the maximum difference was within 6% before the peak load point. Although the load difference between the bonded and unbonded hat sections is apparent throughout the entire loading history, there are two load points which are closely related to the deformation mechanism. The buckling load point represents the structural instability and to some extent determines the consequent load history, and the peak load point is dependent on the buckling mode.

Post-buckling stress distribution tests with the Pressurex® pressure indicating sensor film reveal that, unlike the situation of a thin plate with all simply supported edges, the bonded hat sections had a nearly uniform stress distribution on the cross-section at the peak load point except at the four corners. The unbonded hat sections also had a uniform stress distribution on the face plates, web plates and the flanges
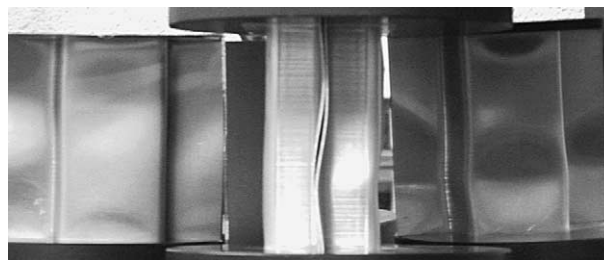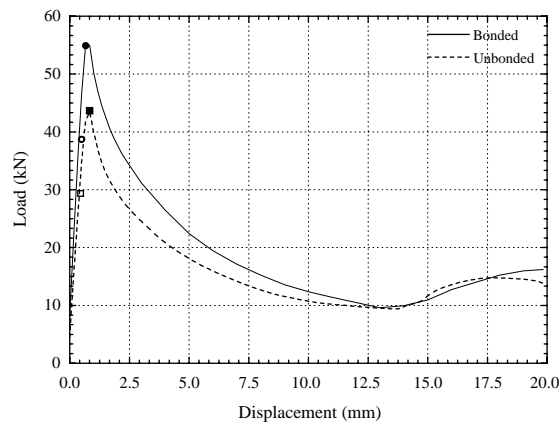

Fig. 6. The 1st anti-symmetric buckling mode of the unbonded hat section at ultimate strength point.

Table 2
Experimental buckling characteristics and ultimate strength of the bonded and unbonded hat sections

Hat sections	Mean buckling load (kN)	Buckling mode	Mean peak load (kN)
Bonded	35.4	Symmetric	53.7
Unbonded	26.1	Anti-symmetric	41.1

□ The 1st bucklingmode load point ofunbonded hatsection

○ The 3rd bucklingmode load point of bonded hat section

■ Peak load point of theunbonded hat section

● Peak load point of the bonded hat section

Fig. 7. Experimental crushing load response comparison between the bonded and unbonded hat sections.

of one of the hat sections, but zero stress on the flanges of the other hat section because these two flanges were already out of contact with the platen when peak load occurred. Similarly, the four corners had lower stress as well due to distortion of the common edges.

Fig. 5 clearly shows that the flanges in the bonded hat sections were not heavily deformed and were almost straight at the peak load point, so that they still carried significant load. However, in the unbonded case, the flanges were no longer straight and out of contact with the loading platen when the peak load was reached as can be seen in Fig. 6, thus, their load carry capability was greatly reduced.

The anti-symmetric 1st and the symmetric 3rd buckling modes in the face plates were simulated using ABAQUS code, and the buckling mode shapes are shown in Figs. 8 and 9 respectively. The buckling mode patterns and the predicted load, together with test results, are listed in Table 3. The difference between predicted buckling load and measured buckling load is expressed by $\delta\%$. The predicted buckling mode correlates with the measured one, and the buckling loads predicted by the finite element analysis are higher than those from the tests, and the agreement can be improved by refining the mesh of the model.

Fig. 8. Finite element simulation of the 1st anti-symmetric buckling mode of the face plate.

Fig. 9. Finite element simulation of the 3rd symmetric buckling mode of the face plate.

Table 3
Finite element buckling prediction of bonded and unbonded hat sections (1200 elements)

Hat sections	Predicted buckling mode	Predicted buckling load (kN)	Experimental mean buckling load (kN)	$\delta\%$
Bonded	Symmetric	41.8	35.4	18.1
Unbonded	Anti-symmetric	28.8	26.1	10.3

A convergence study was carried out in the present work, and Fig. 10 shows that as the degrees of freedom of the entire model increased, the predicted buckling load converged very quickly.

For a very rough evaluation of the hat section's ultimate strength that corresponds to the peak load point, the classical formulae were checked. When the calculation is made, plate members of the hat section have to be computed separately. After the individual calculation, the total summation of each load value yields the ultimate strength of the entire hat section. Both the face and web plate buckling loads were computed using Eq. (6), and the flanges have one edge free so that Eq. (7) was used to computed the flange's strip width c. In order to simplify the calculation, the adhesive layer was neglected. Also, in the unbonded case, two flanges are not in touch with the platen so that only two flanges were considered in the calculation. The calculation results for both bonded and unbonded cases are listed in Table 4. The difference between the calculated and the experimental results is expressed by $\delta\%$.

It can be seen in Table 4 that considerable difference in the ultimate load exists between the classical formulae evaluation and the experimental results. It indicates that due to the differences in the boundary conditions and the practical restraint in the plate members, classical formulae present conservative ultimate load values.

Actually, in Von Karman's ultimate strength assumption expressed in Eq. (5), the two side portions of the rectangular sheet enter the plastic deformation stage whereas the middle part remains elastic. In the hat sections, the practical situation is far more complicated than the assumption. Because there is no constraint that keeps the common edges straight during compression, at the sides of the plate element buckling is not prevented as encountered in simply supported case. Therefore, the stress distribution is different from that
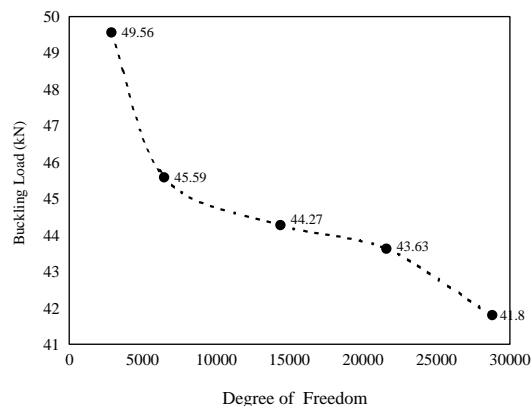

Fig. 10. Convergence study of the predicted buckling load.

Table 4
Ultimate strength (peak load) calculation by classical formulae

Hat sections	Bonded hat section	Unbonded hat section
Flange strip c	11.9 mm	11.9 mm
Face plates P_{ult} ($C = 1.5$)	10.4 kN	10.4 kN
Web plates P_{ult} ($C = 0.95$)	13.2 kN	13.2 kN
Flanges P_{ult}	16.6 kN	8.3 kN
Total hat section P_{ult}	40.2 kN	31.9 kN
Experimental results (mean)	53.7 kN	41.1 kN
$\delta\%$	25.1	22.4

Table 5
Ultimate strength (peak load) calculation by proposed formulae

Hat sections	A or A_{eff} (mm^2)	Results from Eq. (8) or (9) (kN)	Experimental results (kN)	$\delta\%$
Bonded	300	52.5	53.7	2.2
Unbonded	250	43.8	41.1	6.6

of a buckled thin plate with all four edges simply supported. Also, the bonded hat section consists of plate members with different thickness. The flanges do not even buckle when the face plates have reached the yield stress.

To simplify the calculation, we can assume that the entire cross-section of the hat sections reaches σ_y when the ultimate load is reached. The simplified formula here is proposed as

$$P_{ult} = \sigma_y \cdot A \tag{8}$$

where A is the total cross-sectional area of the hat section.

Similarly, in the unbonded case, by eliminating two flanges that are out of surface contact, the formula for calculating the ultimate strength has the similar form

$$P_{ult} = \sigma_y \cdot A_{eff} \tag{9}$$

where A_{eff} is the cross-sectional area of the hat section minus the flanges.

The calculation results by the proposed formulae are listed in Table 5. Again, The difference between the calculated and the experimental results is expressed by $\delta\%$ in the table. It can be seen from Table 5 that the peak load values have been greatly improved compared with those by classic formulae.

Even though some tests were conducted on single rectangular metal plate and metal square tubes (Timoshenko and Gere, 1961), the basic assumption described in Eq. (2) does not have a clear physical meaning, while the proposed formulae mentioned above provide a definite reasoning in the theory of plasticity.

6. Conclusions

The following conclusions can be made from the research conducted here:

1. Due to different flange stiffening effects in the adhesively bonded and unbonded aluminum hat sections, the face plates of the bonded hat sections experience a transformation from the anti-symmetric 1st buckling mode into the symmetric 3rd buckling mode, but the face plates in the unbonded hat sections only exhibit the anti-symmetric 1st buckling mode.

2. At the peak load point, the bonded hat sections have nearly straight flanges that lead to the generation of the 3rd buckling mode on the face plates so that the flanges are still the major load carrying plate elements. In the unbonded case, however, the flanges are so distorted because of the excessive development of the 1st buckling mode that some of them make little contributions to the total load carrying capacity of the hat sections.
3. For the ultimate strength (peak load) evaluation of the hat sections, the proposed formulae simplified the procedure and yielded closer results to the test data than the classic formulae.

Acknowledgements

References

Becker, H., 1957. Handbook of Structural Stability, part II—Buckling of Comp. Elements. National Advisory Committee for Aeronautics, NACA TN 3782.

Bulson, P.S., 1969. The Stability of Flat Plates. American Elsevier Publishing Company, Inc. p. 308.

Fay, P.A., Suthurst, G.D., 1990. Int. J. Adhes. Adhes. 10 (3), 128–138.

Lee, K.Y., Kong, B.S, 2000. J. Adhes. Sci. Technol. 14 (6), 817–832.

McGregor, I.J., et al., 1990. SAE Technical Paper 900796: 1–9.

Peery, D.J., 1949a. Aircraft Structures. McGraw-Hill Book Company, Inc. p. 373.

Peery, D.J., 1949b. Aircraft Structures. McGraw-Hill Book Company, Inc. p. 374.

Peery, D.J., 1949c. Aircraft Structures. McGraw-Hill Book Company, Inc. p. 375.

Timoshenko, S., 1936a. Theory of Elastic Stability. McGraw-Hill Book Company, Inc, New York. p. 395.

Timoshenko, S., 1936b. Theory of Elastic Stability. McGraw-Hill Book Company, Inc., New York. p. 401.

Timoshenko, S., 1936c. Theory of Elastic Stability. McGraw-Hill Book Company, Inc., New York. p. 402.

Timoshenko, S., Gere, J.M., 1961. Theory of Elastic Stability, second ed. McGraw-Hill Book Company, Inc., New York. pp. 419–420.

Von Karman, T., et al., 1932. Trans. ASME 54, 53.